Aerosol Science and Technology

ISSN: (Print) (Online) Journal homepage: www.tandfonline.com/journals/uast20

Complex refractive index of vanillic acid aerosol retrieved from 270–600 nm using aerosol extinction and solution phase absorption measurements

Vahid Hosseinpour Hashemi, Tyler Galpin & Margaret E. Greenslade

To cite this article: Vahid Hosseinpour Hashemi, Tyler Galpin & Margaret E. Greenslade (2024) Complex refractive index of vanillic acid aerosol retrieved from 270–600 nm using aerosol extinction and solution phase absorption measurements, Aerosol Science and Technology, 58:5, 569-583, DOI: 10.1080/02786826.2024.2332636

To link to this article: https://doi.org/10.1080/02786826.2024.2332636

AEROSOL SCIENCE AND TECHNOLOGY
2024, VOL. 58, NO. 5, 569–583
https://doi.org/10.1080/02786826.2024.2332636

Complex refractive index of vanillic acid aerosol retrieved from 270–600 nm using aerosol extinction and solution phase absorption measurements

Vahid Hosseinpour Hashemi*, Tyler Galpin**, and Margaret E. Greenslade

Department of Chemistry, University of New Hampshire, Durham, New Hampshire, USA

ABSTRACT

The complex refractive index of vanillic acid, a component of biomass burning emission, in aerosol form generated by atomization is determined from optical measurements over the wavelength range of 270–600 nm. The aerosol extinction differential optical absorption spectrometer (AE-DOAS) measured the extinction spectrum. In addition, the polydisperse particle size distribution is obtained by the differential mobility analyzer and condensation particle counter. Experimental results combined with Mie theory are utilized to retrieve the real part of the complex refractive index while the outcome of a complementary UV-Vis solution phase absorption experiment is used to determine the imaginary part. The obtained values for the real and imaginary parts across the wavelengths are in the range of 1.43–1.65 and 0.000–0.388, respectively. The dependence of vanillic acid absorption on wavelength is strong at short wavelengths. The absorption Ångström exponent value between 300–500 nm is found to be 5.9 ± 0.6, which agrees with the previously reported values for brown carbon. Comparing the obtained n values of this work with the previously reported values for organic and brown carbon shows good agreement.

ARTICLE HISTORY
Received 22 September 2023
Accepted 3 March 2024

EDITOR
Hans Moosmüller

1. Introduction

Aerosols are liquid or solid particles suspended in a gas. Atmospheric aerosol can directly influence the Earth system's energy balance and change local air quality and visibility by scattering and absorbing electromagnetic radiation. Scattering generally cools the system reflecting incoming solar radiation while absorbing warms the system converting both incoming solar radiation and outgoing terrestrial radiation to heat. The uncertainty on the magnitude of scattering to absorption is a limitation in understanding and predicting human-generated impacts on climate change as well as local air quality, visibility, and atmospheric photochemistry. Further, scattering is common to all aerosol types, but absorption occurs for only specific aerosols. In the entire ultraviolet-visible (UV-Vis) region specific organic carbon (OC) aerosol, especially soot (also referred to as black carbon or BC), which is the product of incomplete combustion at high temperatures, and some mineral dust species absorb (Flores et al. 2014; Bond and Bergstrom 2006; Kahnert, Nousiainen, and Räisänen 2007; Petzold et al. 2009; Myhre et al. 2013; Zhang et al. 2021; Wiegand, Mathews, and Smith 2014). While, only in the UV region, OC aerosol featuring chemicals containing polycyclic-aromatic, phenolic, and acidic functional groups, known as brown carbon (BrC) absorb light (Dinar et al. 2008). BrC is thought to be produced from smoldering low temperature combustion (especially biomass burning plumes), soil particles containing HULIS, and secondary formation in the atmosphere (Hecobian et al. 2010; Graber and Rudich 2006; Myhre et al. 2013; Kanakidou et al. 2005).

Biomass burning aerosol (BBA) have been shown to be 74% of total primary OC aerosol emission (Bond et al. 2004) and the significance of BrC absorption from biomass burning is displayed through interconnections between studies (Lack et al. 2013; Washenfelder et al. 2015; Kirchstetter, Novakov, and Hobbs 2004; Zhao et al. 2019; Zhang et al. 2021). For example, Lack et al. (2013) demonstrated that BrC

CONTACT Margaret E. Greenslade margaret.e.greenslade@gmail.com Formerly of Department of Chemistry, University of New Hampshire, Parsons Hall, 23 Academic Way, Durham, NH, 03824, USA.
*Current affiliation: University of New England, Chemistry Department, Biddeford, Maine, USA.
**Current affiliation: Wilbur Technical Services, Mont Vernon, New Hampshire, USA.

Supplemental data for this article can be accessed online at https://doi.org/10.1080/02786826.2024.2332636.

absorption at $\lambda = 404$ nm is correlated to the biomass burning marker, levoglucosan. Tied to that, Washenfelder et al. (2015) measured the aerosol extinction and UV-Vis spectra of OC solutions to quantify absorption at several discrete wavelengths and showed BrC light absorption is related to the amount of BBA in the southeastern US. Kirchstetter, Novakov, and Hobbs (2004) measured the UV-Vis absorption of OC samples in California ($\lambda = 300$–1000 nm) and estimated a range of 50–80% of the total light absorption from carbonaceous compounds was due to BrC and specifically BBA. Zhao et al. (2019) studied the contribution of BrC to total light absorption and found its contribution is 44% ($\lambda = 405$ nm). Zhang et al. (2021) performed a modeling study finding BrC relative to total carbonaceous is responsible for 33–40% of the absorption ($\lambda = 440$ nm) in Thailand when biomass burning is prevalent. The wavelength of light and location are important variables for light absorption in these cases.

BrC can further be divided into water-soluble (WS) and water-insoluble (WI) categories and applying this to studies of optical properties is illustrated by the following (Liu, Bergin, et al. 2013; Liu et al. 2014; Cheng et al. 2016). High absorption in biomass combustion is related to highly conjugated WI aromatic rings; while absorption related to oxygen and/or nitrogen polar functional groups can lead to some WS characteristics (Chen and Bond 2010). Generally, the absorption of WI-BrC is shown to be greater than WS-BrC (Zhang et al. 2013; Cheng et al. 2016; Zhu et al. 2018; Chen and Bond 2010; Sun, Biedermann, and Bond 2007; Huang et al. 2020). For example, an investigation of BrC characteristics in Beijing, China by Cheng et al. (2016) showed ~60% of its absorption at 365 nm is from WI-OC. While over the Tibetan plateau, Zhu et al. (2018) showed that WI-BrC accounted for 1.5 times higher absorption values than WS-BrC at a wavelength of 365 nm. Furthermore, both Chen and Bond (2010) and Sun, Biedermann, and Bond (2007) used data from their works and works by other groups (Havers et al. 1998; Varga et al. 2001; Hoffer et al. 2006) to conclude WI-OC contributes up to five times more UV-Vis absorption than WS-OC.

In addition to direct *in situ* measurements of aerosol absorption and its value as calculated from extracts of BrC and BBA, several experimental approaches have been used to quantify the refractive index for use in climate modeling. The complex refractive index (CRI) is a wavelength dependent physical property defined as $m(\lambda) = n(\lambda) \pm ik(\lambda)$, where n is the real part, which relates to scattering and k is the imaginary part, which relates to absorption. In our work, the aerosol extinction differential optical absorption spectrometer (AE-DOAS), a White-type optical cell coupled to a UV-Vis spectrometer, is used to measure aerosol extinction from 220 to 1050 nm, and then iterative retrieval of the real part is based on the best fit to Mie theory.

The CRIs can be determined similarly to our work but with different instruments or by other methods. For instance, Jiang et al. (2019) used a White-type cell to measure the light extinction of silica and fly ash aerosol. While, Washenfelder et al. (2015) used broadband cavity-enhanced spectroscopy (BBCES) to measure the extinction of carbonaceous aerosol during a field campaign in the Talladega National Forest in central Alabama, and Schnaiter et al. (2003) used a flow tube extinction spectrometer to measure the extinction of soot aerosol. Moreover, Price, Preston, and Davies (2022) used the single-particle (diameter of 3 to 10 μm) levitation platform along with Mie resonance spectroscopy to retrieve the refractive index of WS-chromophores at $\lambda = 589$ nm based on the model proposed by Bain and Preston (2019). On the other hand, Wex et al. (2009) measured the light scattered by monodisperse, laboratory generated secondary organic aerosol (SOA) with a white-light optical particle spectrometer and estimated the n based on a calibration to other samples. Wex et al. (2009) further refined their results by varying n to convert the scattering signal to particle diameter and comparing the result to the mobility diameter set by a differential mobility analyzer (DMA). Liu, Bergin, et al. (2013) took another approach and measured the CRI for SOA thin films using variable angle ellipsometry; it is not clear if results from this method replicates the characteristics of *in situ* particles (Laskin, Laskin, and Nizkorodov 2015).

Some optical instruments work in a single or several discrete wavelengths while others can cover a wide wavelength range. Here, we highlight the working wavelengths for the instruments used to determine refractive indices in the preceding paragraph. A single wavelength of 638 nm over a path length of 30 m was used by Jiang et al. (2019). The BBCES with three LED sources employed by Washenfelder et al. (2015) covers the wavelengths from 355 to 420 nm. The flow tube extinction spectrometer used by Schnaiter et al. (2003) characterizes the wavelengths from 230–1000 nm and a ~5 m path length. While, the Wex et al. (2009) white-light optical particle spectrometer works in the wavelength range from 250 to 1000 nm, but only a single wavelength ($\lambda = 589$ nm) result was

reported. Liu, Bergin, et al. (2013)'s ellipsometer works from 220 to 1200 nm. The AE-DOAS measures extinction from 220 to 1050 nm with a 19 m path length showing enhanced capability in comparison to other instruments as described here.

Levoglucosan is a known BBA chemical marker, but other chemical compounds, such as vanillic acid ($C_8H_8O_4$), have also been identified (Schauer et al. 2001; Gilardoni et al. 2016). Vanillic acid is found in a variety of trees and in the smoke from forest fires and fireplaces (Zangrando et al. 2013). The concentration of vanillic acid in aerosol is reported to be one of the highest for aromatic acids at up to 6500 ng m^{-3} above mixed Amazon forest litter burning, though typical values are ~10 ng m^{-3} (Wan et al. 2019). Interestingly, the concentration of vanillic acid is even found to be 2–3 ng m^{-3} in urban Beijing (Ren et al. 2018). The presence of vanillic acid and ratio of vanillic acid to other aromatic acids can be used for source identification (Wan et al. 2019). The products of oxidation of vanillin can absorb light (Hawthorne et al. 1989). In addition, OH oxidation of compounds like vanillic acid can contribute to light absorbing HULIS (Tang et al. 2020). On the other hand, vanillic acid does not readily undergo photolysis, thus limiting available pathways (Vione et al. 2019). Unlike levoglucosan, vanillic acid does not dissolve well in water (Zhang, Guo, et al. 2016), but is soluble in methanol or a mixture of methanol and water and thus is considered a WI-BrC compound. Vanillic acid does not take up water up to 95% relative humidity (Mochida and Kawamura 2004). As such, vanillic acid in snow and ice does not degrade and can thus be used for historical studies (Wan et al. 2019). Further, its aerosol optical properties are not impacted by humidity variation.

In most works, the extinction for size-selected, monodisperse aerosol (Chartier and Greenslade 2012; Galpin et al. 2017; Jordan et al. 2015; Saseendran et al. 2020) is used to retrieve refractive indices or as described above the values are reported in a single or several discrete wavelengths; there are a limited number of literature reports for retrieving the refractive index of polydisperse aerosol samples with quantified size distributions at a range of wavelengths (Washenfelder et al. 2015; Bluvshtein et al. 2017; Bluvshtein et al. 2016; He et al. 2018). Another motivation for our work is to take a bottom-up approach with laboratory control to characterizing the fundamental physical property of the CRI for vanillic acid aerosol which can be used beyond climate modeling or when combined with other information may be used to explain top-down measurements like those from field campaigns. It is useful to note that chemically similar compounds have similar CRI. Yet, atmospheric aerosols are chemically complex, and thus our results would need to be combined with other information to fully realize a merging between these two approaches. This is especially true because evidence from field campaigns in Nepal, Amazonia and Tajikistan show only 0.02%, 0.05%, and 0.16% of the OC mass concentration is vanillic acid, respectively (Wan et al. 2017; Binabas et al. 1995; Chen et al. 2022). While, Wan et al. (2017) showed levoglucosan as the most abundant biomass burning marker they quantified it at 2% of the OC mass concentration in Nepal. In this work, the AE-DOAS measured broadband *in situ* extinction from $\lambda = 270$ to 600 nm of polydisperse vanillic acid aerosol generated from an atomizer and dried. Complementary UV-Vis spectrometer absorption measurements for vanillic acid in methanol solutions allow determination of the imaginary part of CRI. Mie theory is utilized to replicate the experimental extinction spectrum *via* best fit minimization retrieval of the real part of CRI while holding the imaginary part of the CRI at the value from the solution phase measurements. The real part of the CRI for our vanillic acid aerosol is then compared with the n values determined for organic aerosol (including secondary), biomass burning aerosol, and ambient aerosol in the overlapping wavelength range and favorable agreement is observed. Our work combines optical methods for robust determination of the CRI for a polydisperse aerosol sample with relevancy to biomass burning.

2. Methods

2.1. Aerosol extinction-differential optical absorption spectrometer (AE-DOAS)

Irrespective of using absorption in the historical name, the extinction of vanillic acid aerosol was measured using our custom AE-DOAS. The AE-DOAS (CMS UV-5000, Cerex Monitoring Solutions, LLC Atlanta, GA, USA), has three parts: a 100-watt continuous duty xenon (Xe) lamp source with the spectral range of 220–1050 nm; a single beam UV-Vis spectrometer with a resolution better than 0.5 nm; and a White-type multi-pass gas cell (Chartier and Greenslade 2012). The gas cell is stainless-steel with an approximate internal volume of 5.8 L. The optical path is defined by one primary and two adjustable secondary concave mirrors, all having the same radius of curvature, to create the variable distance, multi-

pass. The lamp and the spectrometer are connected to the gas cell using fiber optic cables (Ocean Optics QP600-2-SR-BX, Ocean Optics, Orlando, FL, USA). More information about the AE-DOAS design is available in Chartier and Greenslade (2012).

In this work, the wavelength range from 270 to 600 nm is reported because the lamp has greater intensity and more stability between these wavelengths. To have reliable results with an instrument that depends on the light intensity, stability is critical, thus the Xe lamp intensity is monitored. Results showed that during the first 60 min of warm up, the lamp intensity peak shifts to longer wavelengths, but after an hour, it reaches a stable state. To decrease the effect of any remaining variation in the lamp's intensity, several background measurements were taken before introducing the sample. Further, the wavelength calibration of AE-DOAS was tested by measuring the absorbance of acetone in the range from 240–340 nm, which shows agreement to the literature spectrum (Meyrahn et al. 1986).

2.2. Sample preparation and measurements

Solutions were made of 0.1% (w/w) of vanillic acid (TCI, Tokyo Chemical Industry Co., LTD, Tokyo, Japan, 121-34-6) in a mixture of deionized water and methanol (Fisher Chemical, 67-56-1) with a solvent ratio of 9:1, where the small amount of methanol solubilizes the vanillic acid. These solutions were pumped into a Collison-type atomizer where high-pressure, dry, particle-free nitrogen (Airgas NI 300; 4 L min^{-1}) generated a polydisperse-sized aerosol sample (May 1973; Liu and Lee 1975). A custom dryer with Accurel® polypropylene permeable membrane tube (6 mm ID) surrounded by a stainless-steel tube (10 mm ID) both with a length of 165 cm was used. The aerosol sample (0.3 L min^{-1}) inside the permeable membrane flows in the opposite direction to dry, particle-free nitrogen (1 L min^{-1}); the aerosol sample flow rate is held at 0.3 L min^{-1} through the experimental set up. The design of the experimental setup, including the aerosol generation on the left side, is shown in Figure 1.

Following aerosol generation and drying, the polydisperse-sized aerosol sample entered the AE-DOAS and the extinction was measured. The optical path length of 19.51 m was used for all experiments. The aerosol sample was then directed to a differential mobility analyzer (DMA, TSI model 3080 L, TSI Inc., Shoreview, MN, USA) where size separation was achieved based on electrical mobility diameter. The DMA sample and sheath flows set in a 1:10 ratio. Singly charged particles in diameters from 14 to 615 nm were separated. Moreover, doublet and triplet charged particles can be present; therefore, multi charge correction is applied by the Scanning Mobility Particle Sizer (SMPS; the DMA and condensation particle counter (CPC) combined) software to transfer the doublet and triplet particles from the diameter bin of the singlet particles to the related actual diameter bins that represent the true particle diameter and thus its optical properties. The resulting nearly monodisperse aerosol sample entered the CPC (TSI, model 3775, TSI Inc., Shoreview, MN, USA) where particle number concentration was measured as the termination step. The uncertainty of DMA and CPC is ± 10% (McMurry 2000).

2.3. Calculations

In this work, Mie theory was used in conjunction with experimental measurements to determine the complex refractive index (CRI, $m(\lambda) = n(\lambda) + ik(\lambda)$) of vanillic acid. Mie theory based on the measured particle size distribution of aerosol and the complex refractive indices can be used to calculate the extinction of particles at specific wavelengths thus generating an extinction spectrum (Chartier and Greenslade 2012). By changing the refractive index values of n while keeping the k values at the UV-Vis determined value (see below), a program coded in Fortran was used to achieve the best agreement between calculated and experimental extinction spectra.

In addition to the above closure-type refractive index determination with Mie theory, the imaginary part of the refractive index, k, and the absorption Ångström exponent were determined from UV–Vis absorbance. Spectra were acquired for eight solutions of vanillic acid in optically pure methanol with the concentrations of 2.03, 2.07, 2.91, 2.96, 4.85, 4.94, 6.93, and 7.06×10^{-5} M or 3.43, 3.49, 4.90, 4.98, 8.16, 8.31, 11.7, and 11.9×10^{-3} g L^{-1} using a Varian Cary 50 spectrometer; these are proper concentrations to apply Beer-Lambert law. The solvent background absorbance was subtracted. The absorption coefficient was calculated using the following equation:

$$\frac{\alpha_{abs}}{\rho} = 1000 \; ln(10) \frac{A_{abs}}{cl} \tag{1}$$

where α_{abs} is the absorption coefficient in cm^{-1}, ρ is the density in g cm^{-3}, A_{abs} is absorbance, c is concentration in g L^{-1}, and l is the optical path length in cm (Chen and Bond 2010). There is a known solvent

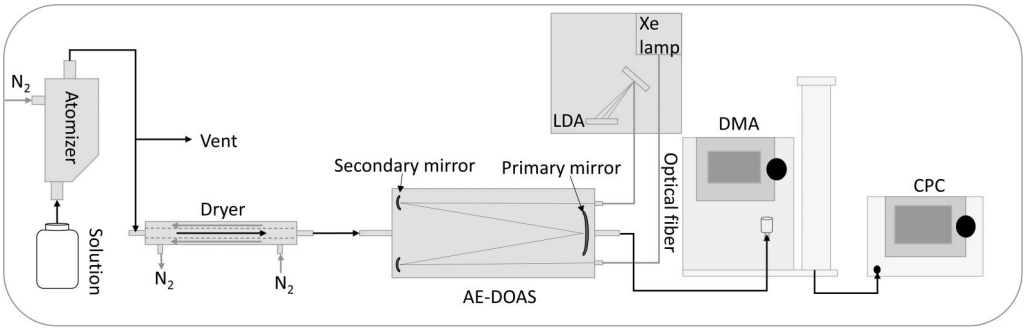

Figure 1. The experimental set up to measure aerosol extinction and size distribution. Black arrows: the direction of aerosol sample movement through the system; grey arrows within the dryer: nitrogen gas flow direction. Aerosol generation is shown (atomizer, dryer) on the left side. The extinction of dried, polydisperse aerosol is measured with the AE-DOAS in the middle. Then, the size distribution of the aerosol sample is measured by DMA in size scanning mode coupled to the CPC determining aerosol number concentration on the right side. (AE-DOAS: aerosol extinction differential optical absorption spectrometer; Xe lamp: xenon lamp; LDA: linear diode array; DMA: differential mobility analyzer; CPC: condensation particle counter).

effect in absorbance spectroscopy and thus measurements of powder sample using a Varian Cary 50 spectrometer equipped with a Barrelino diffuse reflectance probe (barium sulfate ($BaSO_4$) as background) were also made. Using the relation $\alpha_{abs} = 4\pi k/\lambda$, the absorption coefficient is used to determine the imaginary part of the refractive index (Sun, Biedermann, and Bond 2007). Furthermore, the wavelength dependence of absorption can be represented by the following equation:

$$\alpha_{abs} = K \times \lambda^{-AAE} \tag{2}$$

where α_{abs} is absorption coefficient converted to Mm^{-1} (averaged value obtained from 24 UV-Vis measurement of eight different vanillic acid solutions), K is fitting parameter and AAE is absorption Ångström exponent. In the present work, a linear regression between log α_{abs} and log λ in the wavelength range 300–500 nm is used to obtain AAE for the vanillic acid solutions.

3. Results

One of the outcomes is the experimental extinction spectrum of a distribution of vanillic acid aerosol. To obtain the extinction, five scans of light intensities in the presence of dry, filtered and particle-free nitrogen gas as background intensity (I_0), and six scans of aerosol sample (I) are measured by AE-DOAS for each trial. Using Equation (3) and the averaged value of I_0 and I, the extinction, α_{ext} (cm^{-1}), for a particular aerosol sample can be calculated by combining optical information and pathlength of the gas cell (l) in cm:

$$\alpha_{ext} = \frac{-ln\left(\frac{I}{I_0}\right)}{l} \tag{3}$$

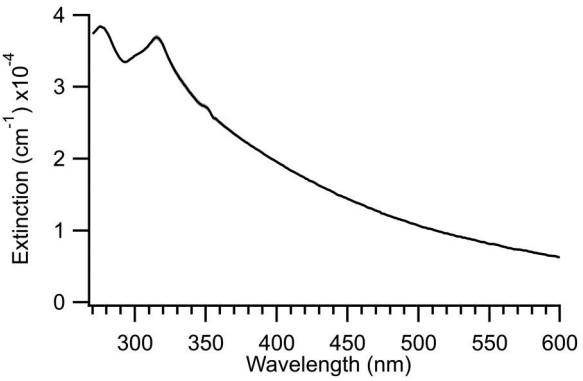

Figure 2. AE-DOAS measured extinction of a distribution of vanillic acid aerosol, smoothed with a 5-point boxcar average as a function of wavelength from 270–600 nm. Error bars representing the standard deviation of six measured scans for a trial were calculated; they are too small to be shown at approximately 10^{-9} to 10^{-10} cm^{-1}.

The obtained average experimental extinction spectrum for one representative trial is illustrated in Figure 2.

In Figure 2, there is an initial and maximum peak at $\lambda = 280$ nm, then a smooth decrease to $\lambda = 294$ nm followed by an increase to a secondary peak at $\lambda = 315$ nm. In addition, there is a fluctuation in the spectrum at wavelengths from 347 to 358 nm related to an instrumental artifact as it is also seen in the background spectra. The best wavelength range of performance for this instrument was reported from 235–700 nm (Chartier and Greenslade 2012). In this work, based on low fluctuations in the obtained background, differences between I_0 and I, and consequently low fluctuations in the experimental extinction, the wavelength range is narrowed to between 270 and 600 nm.

In addition to the extinction spectrum, nine scans of particle size distribution are measured by SMPS for

each trial; there is a difference in the number of scans because of a time difference for each type of measurement. The average particle size distribution for one representative trial is displayed in Figure 3.

As can be seen in Figure 3, vanillic acid particles were quantified in the diameter range 14 to 615 nm with the maximum number concentration at the bin with diameter of 156.8 nm. The number concentration at the maximum is $16{,}000 \pm 2000$ particles cm^{-3} and at the smallest and largest diameters are 5.0 ± 0.5 and 55 ± 6 particles cm^{-3}, respectively.

Mie theory is used to calculate the extinction spectrum from the experimental number concentration of vanillic acid aerosol as a function of diameter, and the CRI at each different wavelength. In the calculation, n is allowed to vary until the best match is obtained and k is a fixed value for each wavelength calculated from UV-Vis spectra measurements as described in the experimental section. This retrieval is repeated over the wavelength range 270–600 nm in 5 nm steps for each trial. The n value is reported as the average from six trials. The averaged k values at 5 nm steps used in the calculation were determined from 24 UV-Vis absorption spectra for eight different vanillic acid solutions using Equation (1), which normalizes for concentration differences (the online supplementary information (SI) Figure S1 shows collected UV-Vis absorbance spectra of vanillic acid in methanol with different concentrations and Figure S2 shows a comparison of this with the absorbance spectra calculated from a measurement of reflectance by a powder sample of vanillic acid). Figure S1 shows there is no shift in absorbance with the change of concentration, however Figure S2 shows the expected blue shift is observed between powder and solution samples of vanillic acid due to the polar solvent. We briefly examine the differences between the two differently collected absorbance spectra in the caption of Figure S2. The solution phase absorbance measurements have been used below because aerosol samples were generated from solution. Because of the detection limit, none of the obtained UV-Vis spectra showed measurable absorption for wavelengths longer than 325 nm; therefore, the k values of vanillic acid are zero or almost zero in these wavelengths. The averaged k values ($N = 24$; standard deviation of the mean) and precision-based 95% confidence interval uncertainties in the range of 270–600 nm are shown in Figure 4.

The k value of the CRI in Figure 4 shows the maximum peak at $\lambda = 270$ nm, then a decrease to a valley at $\lambda = 280$ nm and a secondary peak at $\lambda = 290$ nm. In wavelengths longer than 290 nm, k values decline. Finally, k reaches zero or nearly zero over the wavelengths $\lambda > 325$ nm. These imaginary CRI values are numerically listed in Table 1.

The real part of the CRI, n, is obtained by varying it in Mie calculations to achieve the minimized difference between calculated and experimental extinction at similar wavelengths (where there is a minor wavelength shift of ~0.1 nm between the two methods). This method is applied in the range of 270–600 nm for every 5 nm. The n values are calculated for each of six trials, and the average n value and uncertainty as a function of wavelength is illustrated in Figure 5.

Figure 5 illustrates the highest n values in shorter wavelengths with a general decrease as wavelength

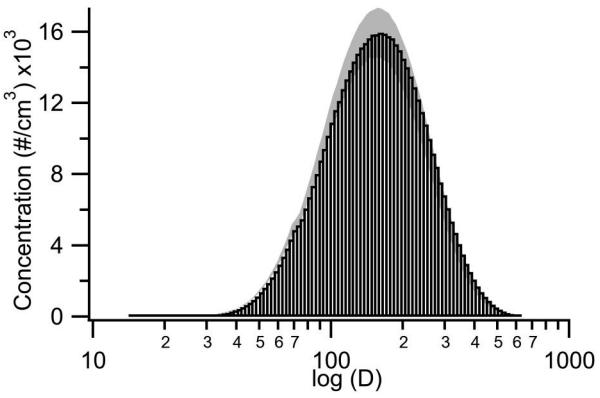

Figure 3. CPC measured number concentration of vanillic acid aerosol as a function of log of particle electric mobility diameter bin controlled with a DMA. The shaded area represents the standard deviation of nine measured scans for the representative trial.

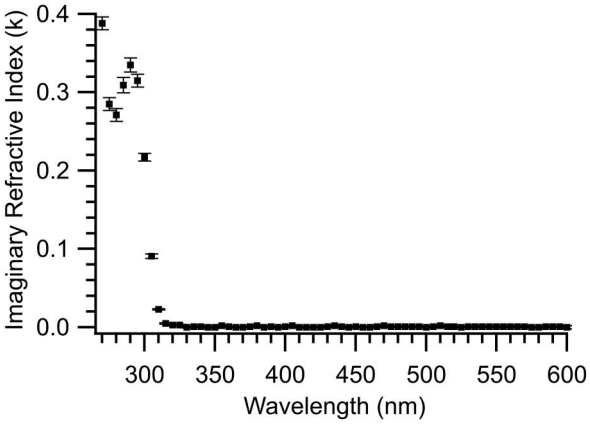

Figure 4. The imaginary part of the CRI, k, as a function of wavelength calculated from absorbance spectra collected with a Cary 50 UV-Vis spectrometer in the range of 270–600 nm. The error bars represent the 95% confidence interval (precision) of 24 standard deviation of the mean calculated k values from eight solutions (three scans per solution). The error bars in the wavelengths above 325 nm are ±0.001. The estimated accuracy of this method for small wavelengths is approximately 8%.

Table 1. The retrieved real, *n*, and calculated imaginary, *k*, parts of CRI values for vanillic acid aerosol in the wavelength range of 270–600 nm. The reported *n* is the average of six retrieved *n* values from best fit Mie theory calculations for six trials. The reported *k* is an average of 24 calculated *k* values using Equation (1) and UV-Vis measurements of eight different vanillic acid solutions in methanol. The uncertainties on the CRI values are the 95% confidence interval.

λ(nm)	n*	k**	λ(nm)	n	k	λ(nm)	n	k
270	1.62(0.06)	0.388(0.008)	385	1.47	0.000	500	1.44	0.000
275	1.65(0.05)	0.285(0.008)	390	1.47	0.001	505	1.44	0.001
280	1.63(0.05)	0.271(0.008)	395	1.47	0.000	510	1.44	0.002
285	1.58(0.04)	0.309(0.010)	400	1.46	0.001	515	1.44	0.001
290	1.53(0.04)	0.335(0.009)	405	1.46	0.002	520	1.44	0.001
295	1.53(0.03)	0.315(0.008)	410	1.46	0.000	525	1.44	0.000
300	1.55(0.03)	0.217(0.005)	415	1.46	0.000	530	1.44	0.001
305	1.54	0.091(0.003)	420	1.46	0.000	535	1.43	0.001
310	1.54	0.023	425	1.46	0.000	540	1.43	0.001
315	1.56	0.005	430	1.45	0.001	545	1.44	0.001
320	1.55	0.003	435	1.45	0.002	550	1.43	0.001
325	1.53	0.003	440	1.45	0.001	555	1.43	0.001
330	1.51	0.000	445	1.45	0.000	560	1.43	0.001
335	1.50	0.001	450	1.45	0.001	565	1.43	0.001
340	1.49	0.001	455	1.45	0.000	570	1.43	0.001
345	1.49	0.000	460	1.45	0.000	575	1.43	0.000
350	***	0.000	465	1.44	0.001	580	1.43	0.000
355	***	0.002	470	1.44	0.002	585	1.43	0.001
360	1.48	0.001	475	1.44	0.001	590	1.43	0.001
365	1.48	0.000	480	1.44	0.001	595	1.43	0.001
370	1.47	0.000	485	1.44	0.001	600	1.43	0.000
375	1.47	0.001	490	1.44	0.001			
380	1.47	0.002	495	1.44	0.001			

*The uncertainty value on *n* is ± 0.02 for $\lambda > 300$ nm except for 545 nm which is ± 0.01.
**The uncertainty value on *k* is ± 0.001 for $\lambda > 305$ nm.
***The *n* values are excluded due to instrumental artifacts at these wavelengths.

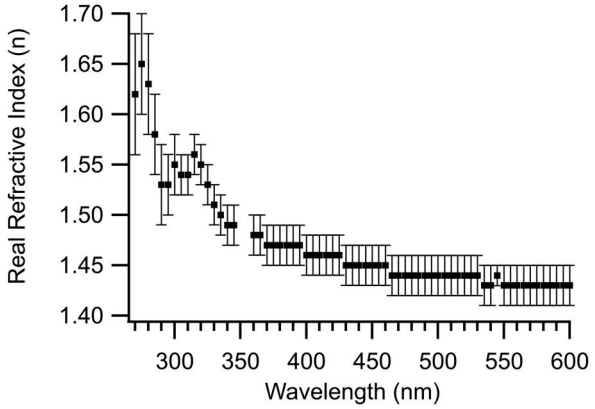

Figure 5. The real part of the CRI, *n*, as a function of wavelength from 270–600 nm as obtained *via* retrieval minimization from fit of Mie theory calculated spectra to experimental extinction spectra. The error bars represent the 95% confidence interval of six *n* values from six trials. The *n* values at 350 and 355 nm are not reported because of instrumental artifacts in that region.

increases. There is a minor increase to a small secondary peak at $\lambda = 315$ nm. The *n* values for 350 and 355 nm were excluded because of an instrumental artifact which increases the uncertainty in the extinction. The retrieved CRI values and uncertainties are given in Table 1.

4. Discussion & conclusions

Figure 2 demonstrates the experimental extinction spectrum with intensity of $\sim$1-4 $\times 10^{-4}$ cm^{-1} for polydisperse vanillic acid aerosol suspended in nitrogen gas in the wavelength range 270–600 nm. The extinction value is higher in shorter wavelengths and declines as energy decreases. Two distinguishable extinction peaks can be noticed at $\lambda = 280$ and 315 nm and the higher energy one shows the greatest extinction value. Besides extinction variability in wavelengths from 347 to 358 nm related to an instrumental error, the spectrum has a smooth decrease to longer wavelengths.

The imaginary, *k*, and real, *n*, parts of CRI as a function of wavelength for the vanillic acid aerosol are shown in Figures 4 and 5, respectively. The detailed numerical values are presented in Table 1. In Figure 4, the obtained *k* value for vanillic acid is between 0.000 and 0.388 in the wavelength range of 270–600 nm. The absolute uncertainty on the *k* value is higher in shorter wavelengths (±0.003–0.008) where the calculated *k* values are higher and vanillic acid shows significant absorption, while there is smaller absolute uncertainty on the *k* value in longer wavelengths (±0.001). Two *k* values related to the detected peaks in the absorption spectra of vanillic acid (Figure S1) are located at $\lambda = 270$ and 290 nm. These two absorption peaks are related to the n $\rightarrow \pi^*$ electronic transitions in the vanillic acid molecule (Santos, Santos, and Duarte 2016). In the wavelengths longer than 290 nm, there is a decline in the *k* value reaching its minimum value (zero or nearly zero) in wavelengths at and longer than 330 nm where there is also no absorption observed in the UV-Vis spectrum. Between wavelengths from 315 to 325 nm, the absorption is small, but it is not zero. This is similar to the absorption behavior of BrC, which shows greater absorption of radiation and thus, higher *k* value at ultraviolet and violet region of the light spectrum with lower or ultimately no absorption when the light energy decreases (Kirchstetter, Novakov, and Hobbs 2004; Hoffer et al. 2006; Moosmüller et al. 2011). Furthermore, using linear regression between log α_{abs} and log λ in the range from 300–500 nm, an AAE value is obtained to investigate the wavelength dependence of vanillic acid absorption (see Figure S3). The obtained AAE value is 5.9 ± 0.6 representing a strong wavelength dependence (AAE > 2) and a sharp

increase of the absorption in shorter wavelengths (Kirchstetter, Novakov, and Hobbs 2004). The obtained AAE is comparable to 5.2–5.3 reported for HULIS-BrC by Huang et al. (2020) in 300–500 nm, 5.7 ± 0.5 for BrC by Jiang et al. (2021) in 330–400 nm and 5.8–5.9 for WI-OC by Wang et al. (2020) in 300–450 nm. It is statistically comparable to the value 4.8 ± 0.9 reported for HULIS by Jiang et al. (2020) in 330–400 nm. The obtained AAE is lower than the reported values 7.2 ± 1.3 for WI-BrC by Ni et al. (2021) in 300–500 nm and 7.10 for methanol extract by Cheng et al. (2016) in 310–450 nm; however, it is higher than the value 4.2 ± 0.4 for BrC reported by Pani et al. (2021) in 370–470 nm. We note the variability in the wavelength regions of reported AAE in the literature in addition to the variability in AAE values. There are some limiting parameters that lead to the reporting of AAE at a variety of wavelengths such as presence of nitrogen containing compounds in the sample with interfering absorption at $\lambda > 500$ nm, limitation in the experimental capabilities for discrete (instead of broadband) wavelength instruments, and selecting the wavelengths based on the linearity of log-log plots.

As mentioned in the experimental section, the multiply charge corrected size distribution should be used in Mie calculations, and this correction is applied by the SMPS's software supplied by TSI, Inc. The supplied multiple charge correction relies on the number of particles in the bin with the largest diameter particles measured being zero; our non-zero averaged value in the largest bin (55 ± 6 particles cm^{-3}) can introduce errors. We have considered the effect of these particles on the calculated extinction values at several wavelengths using the maximum and minimum retrieved n values (see Table S1). The results in Table S1 show that the percent of extinction from the largest bin is $< 0.71\%$. As the number of particles in the largest bin is only 0.01% of the total number of particles; therefore, this bias can be neglected without any major impact on our obtained retrievals. Not only is the bias small, but we believe it is likely that the optical contribution from larger particles than diameters that can be counted with the SMPS would be added, while the optical contribution from the over counting by not performing the multiple charge corrections for particles larger than ~415 nm would be subtracted and these oppositely signed measurement limitations are similar in magnitude thus allowing a reasonable n value to be retrieved.

In Figure 5, the real part, n, represents a normal dispersion between 1.65–1.43 in the wavelength region from 270 to 600 nm; in a normal dispersion, there are higher values at ultraviolet and violet regions and lower values in yellow and orange wavelengths (Bohren and Huffman 1983). Cauchy's equation is an empirical relation between real part of the refractive index and wavelength for a transparent material that describes this normal dispersion; we have calculated the Cauchy coefficients as $A = 1.4275$, $B = 0.0022$ (μm^2) and $C = 0.0012$ (μm^4) based on a fit and show the relationship with the n values in Figure S4. We observe n variations in the UV region of 280–315 nm likely related to the absorption properties of vanillic acid mentioned above. Generally, n smoothly decreases with decreasing energy; however, an exception is seen in the region of higher absorption for vanillic acid in the UV-Vis spectrum. This inconsistency in the dispersion of n values probably is related to presence of absorption which leads to the limited light transmission in comparison to the light intensity in these wavelengths (van de Hulst 1981; Bohren and Huffman 1983). To validate the effect of absorption on the n values, the Kramers-Kronig relation (KK-relation) was applied to calculate the real part of refractive index from the imaginary part following the procedure used by other researchers (Sai et al. 2020). The obtained values from KK-relation are displayed in Figure S4. The comparison between n values experimentally obtained and those calculated from the KK-relation shows generally good agreement; however, some deviation can be seen in the wavelengths from 300–310 nm where the experimental data shows additional structure (two smaller peaks) in comparison the calculated data (single, more intense peak). Greater uncertainty originating from larger difference between obtained n values from each trial is found in the ultraviolet and violet regions compared to that in longer wavelengths. This variation in n values can be related to the greater lamp variability relative to the lower intensity at shorter wavelengths, presence of absorption at shorter wavelengths ($k > 0$), and the larger effect of observed variation in particle size distribution on the calculated extinction values at shorter wavelengths. No n value is reported at $\lambda = 350$ and 355 nm because of an instrumental artifact.

The obtained n values are compared with the literature across the wavelength range studied in this work. Since vanillic acid is an organic molecule and can be one of the components of biomass burning plumes, our results are specifically compared with optical properties of ambient aerosol, biomass burning, dry aerosol and organic molecules (OM) or other BrC

samples. All comparisons discussed below are graphically shown in Figure 6.

The retrieved UV-Vis optical properties of dried ambient aerosol with likely transportation influence were determined by Bluvshtein et al. (2016) using a combination of instruments to measure the extinction and absorption of aerosols in the wavelength range from 300 to 650 nm. Three wavelengths are chosen to make a comparison with our results. Using the data presented in their figure for time series (nighttime hours), the n value retrieved for this time series can be estimated from 1.50–1.65, 1.40–1.45, and 1.35–1.43 at $\lambda = 300$, 450, and 600 nm, respectively, which show an agreement with our retrieved 1.55 ± 0.03, 1.45 ± 0.02 and 1.43 ± 0.02 values at the same wavelengths, respectively. On the other hand, using a single-particle aerosol mass spectrometer equipped with several lasers, Zhang, Bi, et al. (2016) estimated n values in the range of 1.47–1.53 for ambient aerosols sampled in Guangzhou, China at $\lambda = 532$ nm; these samples may include aerosol composed of material other than OM. For comparison, our finding at a similar wavelength is statistically lower value of 1.44 ± 0.02 at 530 nm. In addition, Aldhaif et al. (2018) found n values in the range of 1.50–1.53 for eight defined air mass type samples and 1.52 for organic aerosol over the United States, Canada, the Pacific Ocean, and the Gulf of Mexico at the wavelength 532 nm which are statistically higher than our reported value of 1.44 ± 0.02 at 530 nm (our closest wavelength).

Schmid et al. (2009) proposed a method to quantify the real portion of the complex refractive index of OM as one of the main carbon components of atmospheric aerosols based on data from a field study of Amazonian biomass burning, finding an averaged n value of 1.46 ± 0.02 at $\lambda = 550$ nm for their data series. This value from Schmid et al. is not statistically different from the value of 1.43 ± 0.02 determined in this work at the same wavelength. Zhao, Li, and Zhao (2020) calculated the n value of 1.37–1.51 at $\lambda = 525$ nm for the black carbon-free particles representing OM based on measurements of black carbon-containing particles with the black carbon contribution removed; for comparison, our work retrieved the value of 1.44 ± 0.02 at the same wavelength. Further,

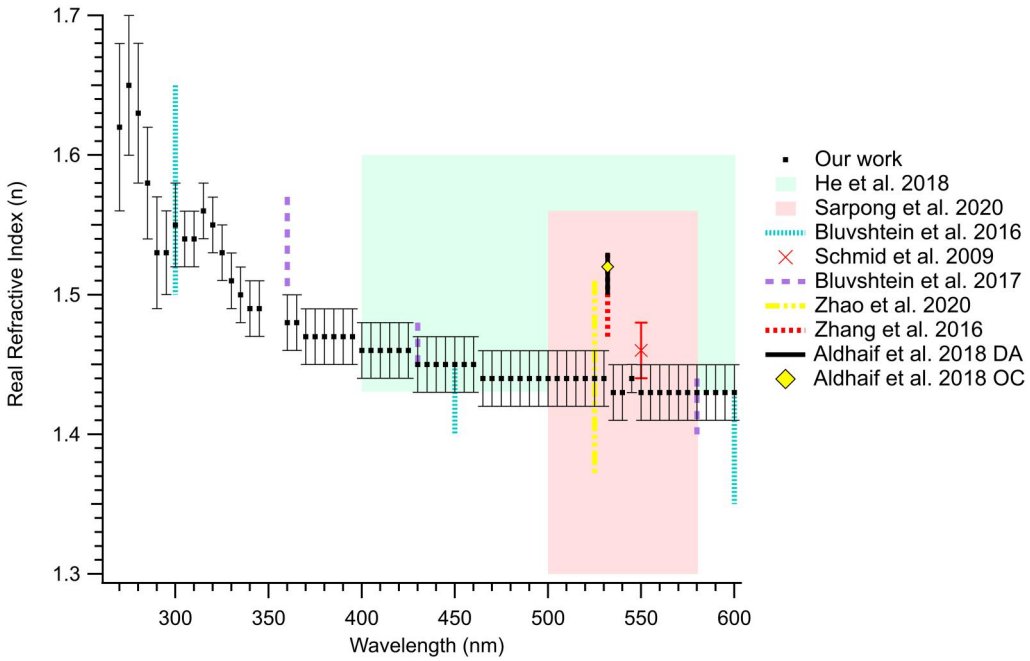

Figure 6. Our retrieved n values for vanillic acid over the wavelength range of 270–600 nm are shown as black solid squares. Retrievals are from extinction measurements using the AE-DOAS where the solution phase UV-Vis absorption measurements are used to constrain the k values. The error bars on n values represent the standard deviation of six n values from six trials. The boxed areas represent the n values reported by He et al. (2018) and Sarpong et al. (2020) over the ranges of 400–600 and 500–580 nm, respectively. The dotted lines illustrate the reported values by Bluvshtein et al. (2016) (only three wavelengths are selected to make a comparison) at 300, 450, and 600 nm. The cross is reported by Schmid et al. (2009) at 550 nm. The long dashed lines express the range of reported n values (only three wavelengths are selected to make a comparison) at 360, 430, and 580 nm by Bluvshtein et al. (2017). The dotted-dashed line is the range of n values at 525 nm reported by Zhao, Li, and Zhao (2020). The short dashed line shows the range of n values at 532 nm reported by Zhang, Bi, et al. (2016). The black line and diamond represent the n values for dry aerosol and organic molecules reported by Aldhaif et al. (2018) at 532 nm.

white light-broadband cavity enhanced spectroscopy was used by He et al. (2018) to retrieve the n value for β-pinene and p-xylene SOA generated with different OH exposures in the range from 1.44 to 1.60 over the wavelengths $400-650$ nm that covers our values ranging from 1.43 to 1.46 from 400–600 nm. In a different study, Bluvshtein et al. (2017) found the broadband optical properties of ambient BBA in Israel in the range of wavelengths from 350 to 650 nm. Again, only three wavelengths are chosen to show a comparison with our data. Using the data they included, the n values retrieved ranged from 1.50–1.57, 1.45–1.48, and 1.40–1.44 for freshly emitted BBA at $\lambda = 360$, 430, and 580 nm, respectively, to allow for comparison with our data. These values can be compared to our values 1.48 ± 0.02, 1.45 ± 0.02, and 1.43 ± 0.02 values at the same wavelengths, respectively. In another study, Sarpong et al. (2020) used the combination of cavity ring-down spectroscopy and nephelometry to retrieve refractive indices of freshly emitted African BBA. The results showed that the n value was in the range of 1.31–1.56 over the range of wavelengths of 500–580 nm, where our work retrieves values fluctuating between 1.43 ± 0.02 and 1.44 ± 0.02 over the same wavelength range.

These differences between our data and ambient aerosol can be related to the composition of samples which is a determining factor in the CRIs. Therefore, knowing the composition of the sample can help to improve understanding of any observed difference; however, the complete chemical characterization of ambient aerosols is not possible due to the complexity. Yet, we observe the n values for organic molecules with similar structures to vanillic acid are reported as 1.5101–1.5425 at 589 nm; however, vanillic acid is not included (Haynes 2016). In addition, the Lorentz and Lorenz equation coupled with density can be used to calculate the n of the CRI for specific chemicals as follows (Bauer, Fajans, and Lewin 1959; Kerker 1969; Dean 1985):

$$r_D = \frac{\left(n_D^2 - 1\right)}{\left(n_D^2 + 2\right)} \frac{1}{\rho} \tag{4}$$

where n_{D} is the real part of refractive index at the sodium D-line, ρ is density and r_{D} specific rotation found by dividing the molar refraction, M_{rD}, by the molar mass. Molar refraction is a function of the chemical makeup of a molecule as well as the types of bonds present. The value is calculated from a standard reference table for atomic and group refractions in Lange's Handbook of Chemistry (Dean 1985). Using Equation (4), density of vanillic acid, 1.2537 g mL^{-1} (Yaws 2014) and the calculated M_{rD} value of 40.247 cm^3 mol^{-1}, the n value was calculated to be 1.51 ± 0.01 at 589 nm. It should be noted that the Lorentz and Lorenz model was empirically derived and previous research has shown a deviation between model and experiment for other organic molecules (Kerker 1969). Further, the CRI observed in this work may be related to the presence of solvent particles in a heterogeneous aerosol sample or solvent remaining on the surface of individual particles. Solvent would likely decrease the retrieved n value as methanol and water are reported to have lower n values of 1.3288 (Haynes 2016) and 1.3329 at $\lambda = 589$ nm, respectively. Based on the above, we can estimate the amount of solvent present as a percentage, using a simple linear combination as: (Ouimette and Flagan 1982)

$$n_{mix} = n_{solvent} \times w_{solvent} + n_{solute} \times w_{solute} \tag{5}$$

where, n_{mix}, n_{solvent} and n_{solute} are the n values for wet generated aerosol sample, solvent (water 9: methanol 1) and solute (vanillic acid, here the value from the Lorentz-Lorenz equation), respectively. The w_{solvent} and w_{solute} represent the fraction of solvent and vanillic acid in a sample, respectively. Equation (5) is used to calculate that the percentage of solvent is $\sim 55 \pm 4\%$. In addition, when comparing our vanillic acid aerosols with results from the field, the chemical complexity and mixing state of the samples from field measurements is directly related to the optical properties including refractive index; thus, highlighting another reason for the observed differences between our work and the literature. Increasing drying time or effectiveness, additional monitoring of humidity in the system, and/or characterizing solvent content (Cai et al. 2016) could further the sample characterization or chemical complexity could be added to aerosol optical property experiments performed with laboratory controls. In addition, future work to better characterize the atomized aerosol sample could be done by other researchers having the necessary equipment and might include quantification of mass changes for a sample on a filter, size changes of single particles using optical tweezers (Bones et al. 2012; Cotterell et al. 2014), the phase of the sample by bound factor determination (Virtanen et al. 2010; Stein et al. 1994; Virtanen et al. 2011; Fischer and Petrucci 2021; Jain and Petrucci 2015), or possibly IR spectroscopy (Cheng et al. 2021; Richards et al. 2020). Furthermore, generating the particles without solvent present would be another option and one we aim to pursue to improve composition control for refractive index determination or retrieval from laboratory-based experiments.

In conclusion, the extinction spectrum of polydisperse vanillic acid aerosols with diameters from 14 to 615 nm was measured using the AE-DOAS in the wavelength range of 270–600 nm. A complementary experiment to measure the UV-Vis absorption of vanillic acid solutions and calculate the imaginary part of CRI was used to constrain the retrievals. Moreover, the wavelength dependence of absorption is studied using obtained AAE value 5.9 ± 0.6 between 300–500 nm, which shows a strong wavelength dependence in shorter wavelengths similar to other BrC studies. Mie theory was used to model and replicate the experimental extinction spectrum. Different n values and a fixed k values (calculated from UV-Vis solution phase measurements) in 5 nm steps were used to minimize the difference between the experimental and calculated extinction spectra. Good agreement between experiment and model was obtained and the resulting CRI values are reasonable. The CRI obtained for vanillic acid aerosol is compared to the literature for organic aerosol (including secondary), biomass burning aerosol, and other ambient aerosol since vanillic acid could be present in a variety of ambient samples. The comparisons showed a strong agreement between the outcomes of this work with the literature. However, some literature identified higher n values than ours. One possible explanation for the higher literature values is the potential for presence of solvent particles mixed in with or on the surface of generated vanillic acid particles due to incomplete solvent removal and we examined this possibility. In addition, the difference in the chemical composition of samples in different works can cause this observed variation in reported n values. One of the motivations for this work is to take a bottom-up approach by characterizing optical properties of a single component aerosol with laboratory control. If multiple sets of bottom-up data are combined, it may be possible to explain and model top-down measurements like those from field campaigns, especially when including our results for regions with biomass burning. Ultimately, if researchers can understand the fundamental reasons for observations, then the uncertainties on the magnitude of aerosol-light interactions can be reduced, and prediction of aerosol's influence on climate change, air quality, visibility and atmospheric photochemistry can be improved. In addition, by performing controlled laboratory optical studies, we are able to improve the general knowledge of the physical and optical properties of chemicals, here for vanillic acid. Our results demonstrate the potential of future applications for the AE-DOAS instrument, specifically in improving the understanding of BBA, OC and BrC optical properties in the atmosphere through the ability to measure the extinction spectrum of *in situ* polydisperse aerosols from 270 to 600 nm.

Acknowledgements

This work was supported by the University of New Hampshire (UNH) Graduate School, College of Engineering and Physical Sciences, Department of Chemistry, and UNH Summer Teaching Assistant Fellowship (STAF) to V.H. V.H. has included a previous version of this work in his doctoral dissertation defended in Spring 2023 and to be published in Summer 2025. Implementation and coding of the Mie Theory model was achieved with the help of Mr. Tod Hagan using original source code from Dr. Sonia Kreidenweis. The authors would also like to thank Dr. Carolyn E. Jordan for her preliminary work to collect and critical observations of the extinction spectra of wet generated vanillic acid aerosol. The authors give special thanks to the reviewers and editor who helped to improve our paper with their keen and insightful questions.

Disclosure statement

The authors declare there is no Complete of Interest at this study.

Funding

This work was funded by the University of New Hampshire, College of Engineering and Physical Sciences, Graduate School and the Department of Chemistry.

ORCID

Vahid Hosseinpour Hashemi http://orcid.org/0000-0001-7303-7814
Margaret E. Greenslade http://orcid.org/0000-0002-2947-2242

References

Aldhaif, A. M., C. Stahl, R. A. Braun, M. A. Moghaddam, T. Shingler, E. Crosbie, P. Sawamura, H. Dadashazar, L. Ziemba, J. L. Jimenez, et al. 2018. Characterization of the real part of dry aerosol refractive index over North America from the surface to 12km. *J. Geophys. Res. Atmospheres.* 123 (15):8283–300. doi:10.1029/2018JD028504.

Bain, A., and T. C. Preston. 2019. Mie scattering from strongly absorbing airborne particles in a photophoretic trap. *J. Appl. Phy.* 125 (9):093101. doi:10.1063/1.5082157.

Bauer, N., K. Fajans, and S. Z. Lewin. 1959. Physical methods of organic chemistry. In *Technique of organic chemistry*, ed. A. Weissberger. New York, NY: Interscience Publishers.

Binabas, M. R., B. R. T. Simoneit, V. Elias, J. A. Cabral, and J. N. Cardoso. 1995. Composition of higher molecular-

weight organic-matter in smoke aerosol from biomass combustion in Amazonia. *Chemosphere.* 30 (5):995–1015. doi:10.1016/0045-6535(94)00442-w.

Bluvshtein, N., J. M. Flores, L. Segev, and Y. Rudich. 2016. A new approach for retrieving the UV-vis optical properties of ambient aerosols. *Atmos. Meas. Tech.* 9 (8):3477–90. doi:10.5194/amt-9-3477-2016.

Bluvshtein, N., P. Lin, J. M. Flores, L. Segev, Y. Mazar, E. Tas, G. Snider, C. Weagle, S. S. Brown, A. Laskin, et al. 2017. Broadband optical properties of biomass-burning aerosol and identification of brown carbon chromophores. *J. Geophys. Res. Atmospheres.* 122 (10):5441–56. doi:10.1002/2016JD026230.

Bohren, C., and D. Huffman. 1983. *Absorption and scattering of light by small particles*. Weinheim Germany: John Wiley & Sons.

Bond, T. C., and R. W. Bergstrom. 2006. Light absorption by carbonaceous particles: An investigative review. *Aerosol Sci. Technol.* 40 (1):27–67. doi:10.1080/02786820500421521.

Bond, T. C., D. G. Streets, K. F. Yarber, S. M. Nelson, J. H. Woo, and Z. Klimont. 2004. A technology-based global inventory of black and organic carbon emissions from combustion. *J. Geophys. Res.* 109, D14203. doi:10.1029/2003JD003697.

Bones, D. L., J. P. Reid, D. M. Lienhard, and U. K. Krieger. 2012. Comparing the mechanism of water condensation and evaporation in glassy aerosol. *Proc. Natl. Acad. Sci. USA.* 109 (29):11613–8. doi:10.1073/pnas.1200691109.

Cai, C., R. E. H. Miles, M. I. Cotterell, A. Marsh, G. Rovelli, A. M. J. Rickards, Y. H. Zhang, and J. P. Reid. 2016. Comparison of methods for predicting the compositional dependence of the density and refractive index of organic-aqueous aerosols. *J. Phys. Chem. A.* 120 (33):6604–17. doi:10.1021/acs.jpca.6b05986.

Chartier, R. T., and M. E. Greenslade. 2012. Initial investigation of the wavelength dependence of optical properties measured with a new multi-pass Aerosol Extinction Differential Optical Absorption Spectrometer (AE-DOAS). *Atmos. Meas. Tech.* 5 (4):709–21. doi:10.5194/amt-5-709-2012.

Chen, P. F., S. C. Kang, L. X. Zhang, S. F. Abdullaev, X. Wan, H. J. Zheng, V. A. Maslov, S. A. Uulu, M. S. Safarov, L. Tripathee, et al. 2022. Organic aerosol compositions and source estimation by molecular tracers in Dushanbe, Tajikistan. *Environ. Pollut.* 302:119055. doi:10.1016/j.envpol.2022.

Chen, Y., and T. C. Bond. 2010. Light absorption by organic carbon from wood combustion. *Atmos. Chem. Phys.* 10 (4):1773–87. doi:10.5194/acp-10-1773-2010.

Cheng, Y., K. B. He, Z. Y. Du, G. Engling, J. M. Liu, Y. L. Ma, M. Zheng, and R. J. Weber. 2016. The characteristics of brown carbon aerosol during winter in Beijing. *Atmos. Environ.* 127:355–64. doi:10.1016/j.atmosenv.2015.12.035.

Cheng, Z. Z., N. Sharma, K. P. Tseng, L. Kovarik, and S. China. 2021. Direct observation and assessment of phase states of ambient and lab-generated sub-micron particles upon humidification. *RSC Adv.* 11 (25):15264–72. doi:10.1039/d1ra02530a.

Chung, S. H., and J. H. Seinfeld. 2005. Climate response of direct radiative forcing of anthropogenic black carbon. *J. Geophys. Res.* 110, D11102. doi:10.1029/2004JD005441.

Cotterell, M. I., B. J. Mason, A. E. Carruthers, J. S. Walker, A. J. Orr-Ewing, and J. P. Reid. 2014. Measurements of the evaporation and hygroscopic response of single fine-mode aerosol particles using a Bessel beam optical trap. *Phys. Chem. Chem. Phys.* 16 (5):2118–28. doi:10.1039/c3cp54368d.

Dean, J. A. 1985. *Lange's handbook of chemistry*. US: McGraw-Hill.

Dinar, E., A. Abo Riziq, C. Spindler, C. Erlick, G. Kiss, and Y. Rudich. 2008. The complex refractive index of atmospheric and model humic-like substances (HULIS) retrieved by a cavity ring down aerosol spectrometer (CRD-AS). *Faraday Discuss.* 137:279–95. doi:10.1039/b703111d.

Fischer, K. B., and G. A. Petrucci. 2021. Utilizing an electrical low-pressure impactor to indirectly probe water uptake via particle bounce measurements. *Atmos. Meas. Tech.* 14 (12):7565–77. doi:10.5194/amt-14-7565-2021.

Flores, J. M., D. F. Zhao, L. Segev, P. Schlag, A. Kiendler-Scharr, H. Fuchs, A. K. Watne, N. Bluvshtein, T. F. Mentel, M. Hallquist, et al. 2014. Evolution of the complex refractive index in the UV spectral region in ageing secondary organic aerosol. *Atmos. Chem. Phys.* 14 (11):5793–806. doi:10.5194/acp-14-5793-2014.

Galpin, T., R. T. Chartier, N. Levergood, and M. E. Greenslade. 2017. Refractive index retrievals for polystyrene latex spheres in the spectral range 220-420 nm. *Aerosol Sci. Technol.* 51 (10):1158–67. doi:10.1080/02786826.2017.1339014.

Gilardoni, S., P. Massoli, M. Paglione, L. Giulianelli, C. Carbone, M. Rinaldi, S. Decesari, S. Sandrini, F. Costabile, G. P. Gobbi, et al. 2016. Direct observation of aqueous secondary organic aerosol from biomass-burning emissions. *Proc. Natl. Acad. Sci. USA.* 113 (36):10013–8. doi:10.1073/pnas.1602212113.

Graber, E. R., and Y. Rudich. 2006. Atmospheric HULIS: How humic-like are they? A comprehensive and critical review. *Atmos. Chem. Phys.* 6 (3):729–53. doi:10.5194/acp-6-729-2006.

Havers, N., P. Burba, J. Lambert, and D. Klockow. 1998. Spectroscopic characterization of humic-like substances in airborne particulate matter. *J. Atmos. Chem.* 29 (1):45–54. doi:10.1023/A:1005875225800.

Hawthorne, S. B., M. S. Krieger, D. J. Miller, and M. B. Mathiason. 1989. Collection and quantitation of methoxylated phenol tracers for atmospheric-pollution from residental wood stoves. *Environ. Sci. Technol.* 23 (4):470–5. doi:10.1021/es00181a013.

Haynes, W. 2016. *Handbook of chemistry and physics: A ready-reference book of chemical and physical data*. Boca Raton, FL: CRC Press.

He, Q. F., N. Bluvshtein, L. Segev, D. Meidan, J. M. Flores, S. S. Brown, W. Brune, and Y. Rudich. 2018. Evolution of the complex refractive index of secondary organic aerosols during atmospheric aging. *Environ. Sci. Technol.* 52 (6):3456–65. doi:10.1021/acs.est.7b05742.

Hecobian, A., X. Zhang, M. Zheng, N. Frank, E. S. Edgerton, and R. J. Weber. 2010. Water-soluble organic aerosol material and the light-absorption characteristics of aqueous extracts measured over the Southeastern United States. *Atmos. Chem. Phys.* 10 (13):5965–77. doi:10.5194/acp-10-5965-2010.

Hoffer, A., A. Gelencsér, P. Guyon, G. Kiss, O. Schmid, G. P. Frank, P. Artaxo, and M. O. Andreae. 2006. Optical properties of humic-like substances (HULIS) in biomass-burning aerosols. *Atmos. Chem. Phys.* 6 (11):3563–70. doi:10.5194/acp-6-3563-2006.

Huang, R. J., L. Yang, J. C. Shen, W. Yuan, Y. Q. Gong, J. Guo, W. J. Cao, J. Duan, H. Y. Ni, C. S. Zhu, et al. 2020. Water-insoluble organics dominate brown carbon in wintertime urban aerosol of China: Chemical characteristics and optical properties. *Environ. Sci. Technol.* 54 (13): 7836–47. doi:10.1021/acs.est.0c01149.

Jacobson, M. Z. 2004. Climate response of fossil fuel and biofuel soot, accounting for soot's feedback to snow and sea ice albedo and emissivity. *J. Geophys. Res.* 109, D21201. doi:10.1029/2004JD004945.

Jain, S., and G. A. Petrucci. 2015. A new method to measure aerosol particle bounce using a cascade electrical low pressure impactor. *Aerosol Sci. Technol.* 49 (6):390–9. doi: 10.1080/02786826.2015.1036393.

Jiang, H. X., J. Li, D. H. Chen, J. Tang, Z. N. Cheng, Y. Z. Mo, T. Su, C. G. Tian, B. Jiang, Y. H. Liao, et al. 2020. Biomass burning organic aerosols significantly influence the light absorption properties of polarity-dependent organic compounds in the Pearl River Delta Region, China. *Environ. Int.* 144:106079. doi:10.1016/j.envint.2020.

Jiang, H. , J. Li, R. Sun, G. Liu, C. Tian, J. Tang, Z. Cheng, S. Zhu, G. Zhong, X. Ding, et al. 2021. Determining the sources and transport of brown carbon using radionuclide tracers and modeling. *J. Geophys. Res. Atmospheres.* 126 (9):e2021JD034616. doi:10.1029/2021JD034616.

Jiang, M., X. W. Liu, D. Chen, J. K. Han, Z. F. Wang, and M. H. Xu. 2019. Light extinction method for measuring a low particle concentration with White cell optics: Relationship between light transmittance and particle properties. *Energy Fuels.* 33 (11):12063–72. doi:10.1021/acs.energyfuels.9b02749.

Jones, G. S., A. Jones, D. L. Roberts, P. A. Stott, and K. D. Williams. 2005. Sensitivity of global-scale climate change attribution results to inclusion of fossil fuel black carbon aerosol. *Geophys. Res. Lett.* 32, L14701. doi:10.1029/2005GL023370.

Jordan, C. E., B. E. Anderson, A. J. Beyersdorf, C. A. Corr, J. E. Dibb, M. E. Greenslade, R. F. Martin, R. H. Moore, E. Scheuer, M. A. Shook, et al. 2015. Spectral aerosol extinction (SpEx): A new instrument for in situ ambient aerosol extinction measurements across the UV/visible wavelength range. *Atmos. Meas. Tech.* 8 (11):4755–71. doi:10.5194/amt-8-4755-2015.

Kahnert, M., T. Nousiainen, and P. Räisänen. 2007. Mie simulations as an error source in mineral aerosol radiative forcing calculations. *Quart. J. Royal Meteoro. Soc.* 133 (623):299–307. doi:10.1002/qj.40.

Kanakidou, M., J. H. Seinfeld, S. N. Pandis, I. Barnes, F. J. Dentener, M. C. Facchini, R. Van Dingenen, B. Ervens, A. Nenes, C. J. Nielsen, et al. 2005. Organic aerosol and global climate modelling: A review. *Atmos. Chem. Phys.* 5 (4):1053–123. doi:10.5194/acp-5-1053-2005.

Kerker, M. 1969. *The scattering of light and other electromagnetic radiation*. New York, NY: Academic Press.

Kirchstetter, T. W., T. Novakov, and P. V. Hobbs. 2004. Evidence that the spectral dependence of light absorption by aerosols is affected by organic carbon. *J. Geophys. Res. Atmospheres* 109, D21208. doi:10.1029/2004JD004999.

Lack, D. A., R. Bahreini, J. M. Langridge, J. B. Gilman, and A. M. Middlebrook. 2013. Brown carbon absorption linked to organic mass tracers in biomass burning particles. *Atmos. Chem. Phys.* 13 (5):2415–22. doi:10.5194/acp-13-2415-2013.

Laskin, A., J. Laskin, and S. A. Nizkorodov. 2015. Chemistry of atmospheric brown carbon. *Chem. Rev.* 115 (10):4335–82. doi:10.1021/cr5006167.

Liu, B. Y. H., and K. W. Lee. 1975. Aerosol generator of high stability. *Am. Ind. Hyg. Assoc. J.* 36 (12):861–5. doi: 10.1080/0002889758507357.

Liu, J. M., E. Scheuer, J. Dibb, L. D. Ziemba, K. L. Thornhill, B. E. Anderson, A. Wisthaler, T. Mikoviny, J. J. Devi, M. Bergin, et al. 2014. Brown carbon in the continental troposphere. *Geophys. Res. Lett.* 41 (6):2191–5. doi:10.1002/2013GL058976.

Liu, J., M. Bergin, H. Guo, L. King, N. Kotra, E. Edgerton, and R. J. Weber. 2013. Size-resolved measurements of brown carbon in water and methanol extracts and estimates of their contribution to ambient fine-particle light absorption. *Atmos. Chem. Phys.* 13 (24):12389–404. doi: 10.5194/acp-13-12389-2013.

Liu, P. F., Y. Zhang, and S. T. Martin. 2013. Complex refractive indices of thin films of secondary organic materials by spectroscopic ellipsometry from 220 to 1200 nm. *Environ. Sci. Technol.* 47 (23):13594–601. doi:10.1021/es403411e.

May, K. 1973. The Collison nebulizer: Description, performance and application. *J. Aerosol Sci.* 4 (3):235–43. doi:10.1016/0021-8502(73)90006-2.

McMurry, P. H. 2000. A review of atmospheric aerosol measurements. *Atmospheric Environment* 34 (12–14): 1959–99. doi:10.1016/S1352-2310(99)00455-0.

Meyrahn, H., J. Pauly, W. Schneider, and P. Warneck. 1986. Quantum yields for the photodissociation of acetone in air and an estimate for the life time of acetone in the lower troposphere. *J. Atmos. Chem.* 4 (2):277–91. doi:10.1007/BF00052006.

Mochida, M., and K. Kawamura. 2004. Hygroscopic properties of levoglucosan and related organic compounds characteristic to biomass burning aerosol particles. *J. Geophys. Res.* 109, D21202. doi:10.1029/2004JD004962.

Moosmüller, H., R. K. Chakrabarty, K. M. Ehlers, and W. P. Arnott. 2011. Absorption Angstrom coefficient, brown carbon, and aerosols: Basic concepts, bulk matter, and spherical particles. *Atmos. Chem. Phys.* 11 (3):1217–25. doi:10.5194/acp-11-1217-2011.

Myhre, G., C. E. Lund Myhre, B. H. Samset, and T. Storelvmo. 2013. Aerosol and their relation to global climate and climate sensitivity. *Nature Education Knowledge* 4 (5):7.

Ni, H. Y., R. J. Huang, S. M. Pieber, J. C. Corbin, G. Stefenelli, V. Pospisilova, F. Klein, M. Gysel-Beer, L. Yang, U. Baltensperger, et al. 2021. Brown carbon in primary and aged coal combustion emission. *Environ. Sci. Technol.* 55 (9):5701–10. doi:10.1021/acs.est.0c08084.

Ouimette, J. R., and R. C. Flagan. 1982. The extinction coefficient of multicomponent aerosols. *Atmos. Environ.* 16 (10):2405–19. doi:10.1016/0004-6981(82)90131-7.

Pani, S. K., N. H. Lin, S. M. Griffith, S. Chantara, C. T. Lee, D. Thepnuan, and Y. I. Tsai. 2021. Brown carbon light absorption over an urban environment in northern peninsular Southeast Asia. *Environ. Pollut.* 276. doi:10.1016/j.envpol.2021.116735.

Petzold, A., K. Rasp, B. Weinzierl, M. Esselborn, T. Hamburger, A. Dörnbrac, K. Kandler, L. Schütz, P. Knippertz, M. Fiebig, et al. 2009. Saharan dust absorption and refractive index from aircraft-based observations during SAMUM 2006. *Tellus Series B-Chem. Phys. Meteorol.* 61 (1):118–30. doi:10.1111/j.1600-0889.2008.00383.x.

Price, C. L., T. C. Preston, and J. F. Davies. 2022. Hygroscopic growth, phase morphology, and optical properties of model aqueous brown carbon aerosol. *Environ. Sci. Technol.* 56 (7):3941–51. doi:10.1021/acs.est.1c07356.

Ren, H., M. J. Kang, L. J. Ren, Y. Zhao, X. L. Pan, S. Y. Yue, L. J. Li, W. Y. Zhao, L. F. Wei, Q. R. Xie, et al. 2018. The organic molecular composition, diurnal variation, and stable carbon isotope ratios of PM2.5 in Beijing during the 2014 APEC summit. *Environ. Pollut.* 243 (Pt B):919–28. doi:10.1016/j.envpol.2018.08.094.

Richards, D. S., K. L. Trobaugh, J. Hajek-Herrera, and R. D. Davis. 2020. Dual-balance electrodynamic trap as a microanalytical tool for identifying gel transitions and viscous properties of levitated aerosol particles. *Anal. Chem.* 92 (4):3086–94. doi:10.1021/acs.analchem.9b04487.

Sai, T. Q., M. Saba, E. R. Dufresne, U. Steiner, and B. D. Wilts. 2020. Designing refractive index fluids using the Kramers-Kronig relations. *Faraday Discuss.* 223 (0):136–44. doi:10.1039/d0fd00027b.

Santos, G., P. S. M. Santos, and A. C. Duarte. 2016. Vanillic and syringic acids from biomass burning: Behaviour during Fenton-like oxidation in atmospheric aqueous phase and in the absence of light. *J. Hazard. Mater.* 313:201–8. doi:10.1016/j.jhazmat.2016.04.006.

Sarpong, E., D. Smith, R. Pokhrel, M. N. Fiddler, and S. Bililign. 2020. Refractive indices of biomass burning aerosols obtained from African biomass fuels using RDG approximation. *Atmosphere.* 11 (1):62. doi:10.3390/atmos11010062.

Saseendran, A., S. Mathai, S. Joshi, A. Pakkattil, T. Capek, G. Kinney, C. Mazzoleni, and R. Varma. 2020. Dual-cavity spectrometer for monitoring broadband light extinction by atmospheric aerosols. *Aerosol Sci. Technol.* 54 (10):1183–96. doi:10.1080/02786826.2020.1763249.

Schauer, J. J., M. J. Kleeman, G. R. Cass, and B. R. T. Simoneit. 2001. Measurement of emissions from air pollution sources. 3. C-1-C-29 organic compounds from fireplace combustion of wood. *Environ. Sci. Technol.* 35 (9):1716–28. doi:10.1021/es001331e.

Schmid, O., D. Chand, E. Karg, P. Guyon, G. P. Frank, E. Swietlicki, and M. O. Andreae. 2009. Derivation of the density and refractive index of organic matter and elemental carbon from closure between physical and chemical aerosol properties. *Environ. Sci. Technol.* 43 (4):1166–72. doi:10.1021/es800570p.

Schnaiter, M., H. Horvath, O. Möhler, K.-H. Naumann, H. Saathoff, and O. W. Schöck. 2003. UV-VIS-NIR spectral optical properties of soot and soot-containing aerosols. *J. Aerosol Sci.* 34 (10):1421–44. doi:10.1016/S0021-8502(03)00361-6.

Stein, S. W., B. J. Turpin, X. P. Cai, C. P. F. Huang, and P. H. McMurry. 1994. Measurements of relative humidity-dependent bounce and density for atmospheric particles using the DMA-impactor technique. *Atmos. Environ.* 28 (10):1739–46. doi:10.1016/1352-2310(94)90136-8.

Sun, H., L. Biedermann, and T. C. Bond. 2007. Color of brown carbon: A model for ultraviolet and visible light absorption by organic carbon aerosol. *Geophys. Res. Lett.* 34, L17813. doi:10.1029/2007GL029797.

Tang, S. S., F. H. Li, N. T. Tsona, C. Y. Lu, X. F. Wang, and L. Du. 2020. Aqueous-phase photooxidation of vanillic acid: A potential source of humic-like substances (HULIS). *ACS Earth Space Chem.* 4 (6):862–72. doi:10.1021/acsearthspacechem.0c00070.

van de Hulst, H. C. 1981. *Light scattering by small particles*. Mineola, NY: Dover Publications.

Varga, B., G. Kiss, I. Ganszky, A. Gelencsér, and Z. Krivácsy. 2001. Isolation of water-soluble organic matter from atmospheric aerosol. *Talanta.* 55 (3):561–72. doi:10.1016/s0039-9140(01)00446-5.

Vione, D., A. Albinet, F. Barsotti, M. Mekic, B. Jiang, C. Minero, M. Brigante, and S. Gligorovski. 2019. Formation of substances with humic-like fluorescence properties, upon photoinduced oligomerization of typical phenolic compounds emitted by biomass burning. *Atmos. Environ.* 206:197–207. doi:10.1016/j.atmosenv.2019.03.005.

Virtanen, A., J. Joutsensaari, T. Koop, J. Kannosto, P. Yli-Pirilä, J. Leskinen, J. M. Mäkelä, J. K. Holopainen, U. Pöschl, M. Kulmala, et al. 2010. An amorphous solid state of biogenic secondary organic aerosol particles. *Nature.* 467 (7317):824–7. doi:10.1038/nature09455.

Virtanen, A., J. Kannosto, H. Kuuluvainen, A. Arffman, J. Joutsensaari, E. Saukko, L. Hao, P. Yli-Pirilä, P. Tiitta, J. K. Holopainen, et al. 2011. Bounce behavior of freshly nucleated biogenic secondary organic aerosol particles. *Atmos. Chem. Phys.* 11 (16):8759–66. doi:10.5194/acp-11-8759-2011.

Wan, X., K. Kawamura, K. Ram, S. C. Kang, M. Loewen, S. P. Gao, G. M. Wu, P. Q. Fu, Y. L. Zhang, H. Bhattarai, et al. 2019. Aromatic acids as biomass-burning tracers in atmospheric aerosols and ice cores: A review. *Environ. Pollut.* 247:216–28. doi:10.1016/j.envpol.2019.01.028.

Wan, X., S. C. Kang, Q. L. Li, D. Rupakheti, Q. G. Zhang, J. M. Guo, P. F. Chen, L. Tripathee, M. Rupakheti, A. K. Panday, et al. 2017. Organic molecular tracers in the atmospheric aerosols from Lumbini, Nepal, in the northern Indo-Gangetic Plain: Influence of biomass burning. *Atmos. Chem. Phys.* 17 (14):8867–85. doi:10.5194/acp-17-8867-2017.

Wang, Y. J., M. Hu, N. Xu, Y. H. Qin, Z. J. Wu, L. W. Zeng, X. F. Huang, and L. Y. He. 2020. Chemical composition and light absorption of carbonaceous aerosols emitted from crop residue burning: Influence of combustion efficiency. *Atmos. Chem. Phys.* 20 (22):13721–34. doi:10.5194/acp-20-13721-2020.

Washenfelder, R. A., A. R. Attwood, C. A. Brock, H. Guo, L. Xu, R. J. Weber, N. L. Ng, H. M. Allen, B. R. Ayres, K. Baumann, et al. 2015. Biomass burning dominates

brown carbon absorption in the rural southeastern United States. *Geophys. Res. Lett.* 42 (2):653–64. doi:10.1002/2014GL062444.

Wex, H., M. D. Petters, C. M. Carrico, E. Hallbauer, A. Massling, G. R. McMeeking, L. Poulain, Z. Wu, S. M. Kreidenweis, and F. Stratmann. 2009. Towards closing the gap between hygroscopic growth and activation for secondary organic aerosol: Part 1-Evidence from measurements. *Atmos. Chem. Phys.* 9 (12):3987–97. doi:10.5194/acp-9-3987-2009.

Wiegand, J. R., L. D. Mathews, and G. D. Smith. 2014. A UV-Vis photoacoustic spectrophotometer. *Anal. Chem.* 86 (12):6049–56. doi:10.1021/ac501196u.

Yaws, C. L. 2014. *Thermophysical properties of chemicals and hydrocarbons*. 2nd ed. Waltham, MA: Elsevier.

Zangrando, R., E. Barbaro, P. Zennaro, S. Rossi, N. M. Kehrwald, J. Gabrieli, C. Barbante, and A. Gambaro. 2013. Molecular markers of biomass burning in Arctic aerosols. *Environ. Sci. Technol.* 47 (15):8565–74. doi:10.1021/es400125r.

Zhang, G. H., X. H. Bi, N. Qiu, B. X. Han, Q. H. Lin, L. Peng, D. H. Chen, X. M. Wang, P. A. Peng, G. Y. Sheng, et al. 2016. The real part of the refractive indices and effective densities for chemically segregated ambient aerosols in Guangzhou measured by a single-particle aerosol mass spectrometer. *Atmos. Chem. Phys.* 16 (4):2631–40. doi:10.5194/acp-16-2631-2016.

Zhang, X. L., Y. H. Lin, J. D. Surratt, and R. J. Weber. 2013. Sources, composition and absorption Angstrom exponent of light-absorbing organic components in aerosol extracts from the Los Angeles basin. *Environ. Sci. Technol.* 47 (8):3685–93. doi:10.1021/es305047b.

Zhang, Y. Q., F. Guo, Q. Cui, M. Y. Lu, X. L. Song, H. J. Tang, and Q. S. Li. 2016. Measurement and correlation of the solubility of vanillic acid in eight pure and water plus ethanol mixed solvents at temperatures from (293.15 to 323.15) K. *J. Chem. Eng. Data.* 61 (1):420–9. doi:10.1021/acs.jced.5b00619.

Zhang, Y., Y. Peng, W. Song, Y.-L. Zhang, P. Ponsawansong, T. Prapamontol, and Y. Wang. 2021. Contribution of brown carbon to the light absorption and radiative effect of carbonaceous aerosols from biomass burning emissions in Chiang Mai, Thailand. *Atmos. Environ.* 260:118544. doi:10.1016/j.atmosenv.2021.118544.

Zhao, G., F. Li, and C. S. Zhao. 2020. Determination of the refractive index of ambient aerosols. *Atmos. Environ.* 240: 117800. doi:10.1016/j.atmosenv.2020.117800.

Zhao, Z. Z., J. J. Cao, J. D. Chow, J. G. Watson, A. L. W. Chen, X. L. Wang, Q. Y. Wang, J. Tian, Z. X. Shen, C. S. Zhu, et al. 2019. Multi-wavelength light absorption of black and brown carbon at a high-altitude site on the Southeastern margin of the Tibetan Plateau, China. *Atmos. Environ.* 212:54–64. doi:10.1016/j.atmosenv.2019.05.035.

Zhu, C. S., J. J. Cao, R. J. Huang, Z. X. Shen, Q. Y. Wang, and N. N. Zhang. 2018. Light absorption properties of brown carbon over the southeastern Tibetan Plateau. *Sci. Total Environ.* 625:246–51. doi:10.1016/j.scitotenv.2017.12.183.